Coumarin derivatives as fibronectin-binding protein A inhibitors against bone and joint infections by *Staphylococcus aureus*: Molecular docking and pharmacological profiling

Thu Minh Nguyen, Luan Luong Chu*

National Key Laboratory of Enzyme and Protein Technology, Faculty of Biology, University of Science, Vietnam National University - Hanoi, 334 Nguyen Trai Street, Thanh Xuan Ward, Hanoi, Vietnam

Received 12 August 2025; revised 25 October 2025; accepted 4 April 2026

Abstract:

Bone and joint infections remain a serious clinical problem, with *Staphylococcus aureus* being one of the causative agents. A key factor in the early stage of infection is fibronectin-binding protein A (FnBP-A), which mediates bacterial adhesion to host fibronectin in the extracellular matrix. The increasing prevalence of antibiotic-resistant *S. aureus*, particularly methicillin-resistant strains (MRSA), highlights the need for alternative therapeutic strategies targeting bacterial adhesion. Coumarins have attracted attention as potential antimicrobial agents because of their broad biological activities and reported anti-*S. aureus* effects. In this study, selected coumarin derivatives were evaluated for their inhibitory potential against the FnBP-A-fibronectin complex using molecular docking with AutoDock Vina and AutoDock4. Compounds with favourable binding profiles were further assessed for predicted pharmacological properties. Among the tested compounds, frutinone A and phyllocoumarin showed stronger docking affinities than vancomycin HCl, a commonly used antibiotic for *S. aureus*-associated bone and joint infections. In addition, pharmacological predictions supported their potential for further investigation. These findings suggest that coumarin derivatives, particularly frutinone A and phyllocoumarin, may serve as promising candidates for the development of anti-adhesive agents against *S. aureus*-related bone and joint infections.

*Corresponding author: Email: luancl@vnu.edu.vn

Keywords: **bone and joint infections, coumarins, fibronectin-binding protein A, molecular docking, pharmacological analysis, septic arthritis, *Staphylococcus aureus.***
Classification numbers: **3.5, 3.6**

1. Introduction

Staphylococcus aureus is a major pathogenic agent causing bone and joint infections. Its surface expresses MSCRAMMs that mediate adhesion to osteoblasts, initiating infection [1-3]. Among these, fibronectin-binding proteins A and B (FnBP-A and FnBP-B) interact with fibronectin via a β-zipper mechanism, exposing integrin-binding domains and enabling attachment to α5β1 integrins on osteoblasts [4]. However, the rate of antibiotic resistance in *S. aureus* has increased significantly in recent years. However, antibiotic resistance in *S. aureus* has increased significantly in recent years. According to N.V. An et al. (2024) [5], resistance rates were highest for azithromycin, erythromycin, and clindamycin (≈82%), while remaining low for vancomycin (2.92%). The study also highlighted the high prevalence of methicillin-resistant *S. aureus* (MRSA) and multidrug-resistant *S. aureus* (MDR) reached 73.02% and 60.90%, respectively [5]. These alarming statistics underscore the urgent need to develop new antimicrobial agents with improved efficacy to combat the emergence and spread of drug-resistant *S. aureus* strains.

A study by D.S. Reddy, et al. (2018) [6] showed that novobiocin, an aminocoumarin derivative, inhibits the GyrB subunit of DNA gyrase, thereby disrupting DNA replication in *S. aureus*. These findings highlight the potential of coumarin-based compounds as antimicrobial agents. Coumarin (1,2-benzopyrone), a natural secondary metabolite found in plants, microbes, and fungi, was first isolated from *Dipteryx odorata* by Vogel in 1920 [7]. With its aromatic lactone structure, coumarin can readily participate in chemical reactions to form a wide variety of bioactive derivatives. These derivatives exhibit antioxidant, antifungal, and anti-inflammatory activities, highlighting their pharmacological potential [8-10]. Previous studies have also indicated that coumarin can enhance oral bioavailability [11] and improve the pharmacological activity of parent drugs [12].

Simple coumarins act as precursors to more complex derivatives found in nature. Compounds such as aculeatin, cichoriin, esculin, fraxin, and osthole exhibit anti-inflammatory, antioxidant, antibacterial, and anticancer activities [13-19], while oxime derivatives 3A and 3E show antitubercular activity [6]. Other derivatives also display notable bioactivities, including calophyllolide with anti-inflammatory and wound-healing effects [20], chartreusin with anticancer potential [21], frutinone A with antibacterial activity [22], and hydrangenol with anti-allergic and antioxidant properties [23]. Although phyllocoumarin remains less explored, its structural features make it a promising candidate for in silico evaluation. In this study, selected coumarin compounds were screened and evaluated *in silico* for their potential to inhibit the binding complex between fibronectin-binding protein A (FnBP-A), located on the extracellular matrix of *S. aureus*, and fibronectin present in the host organism.

2. Materials and methods

2.1. Fibronectin-binding protein A (FnBP-A)-fibronectin complex selection

FnBP-A on the surface of *S. aureus* mediates attachment to host cells via intrinsically disordered FnBR regions that bind fibronectin modules, forming stable complexes. Representative complex structures (PDB IDs: 2RKY, 2RKZ, 3CAL, and 2RL0) [24] were selected from the Protein Data Bank (https://www.rcsb.org/). The structural files were downloaded in PDB format, realigned using BIOVIA Discovery Studio 2024 Client 24.1 (Dassault Systèmes) [25], and subsequently converted into PDBQT format for molecular docking

2.2. Binding site identification

The predicted binding coordinates between FnBP-A and fibronectin in all four models (PDB IDs: 2RKZ, 2RKY, 3CAL, and 2RL0) were identified using the PrankWeb server (ELIXIR) [26].

2.3. Ligand preparation

The selection of coumarin compounds was based on their previously reported antibacterial and anti-inflammatory activities. A total of fourteen compounds were selected for analysis (Table 1).

Table 1. Structures of 14 coumarin derivative compounds.

No.	Name	PubChem CID	2D structure	Molecular formula
1	Coumarin	323	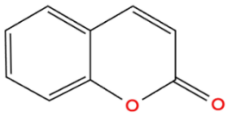	$C_9H_6O_2$
2	Aculeatin	5316354	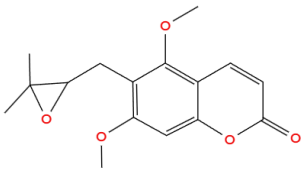	$C_{16}H_{18}O_5$
3	Cichoriin	442101	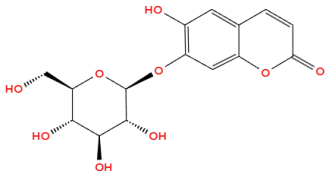	$C_{15}H_{16}O_9$
4	Esculin	5281417	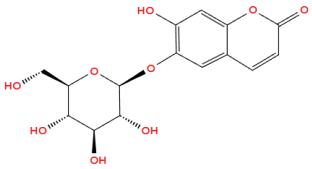	$C_{15}H_{16}O_9$
5	Fraxin	5273567	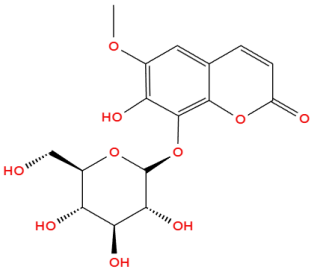	$C_{16}H_{18}O_{10}$
6	Osthole	10228	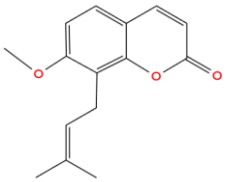	$C_{15}H_{16}O_3$

7	Oximes 3A	120586	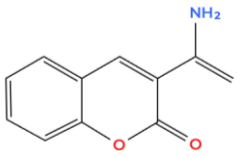	$C_{10}H_7NO_3$
8	Oximes 3E	442935	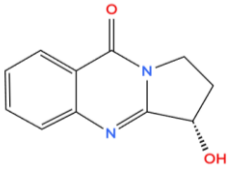	$C_{11}H_{10}N_2O_2$
9	Novobiocin	54675769	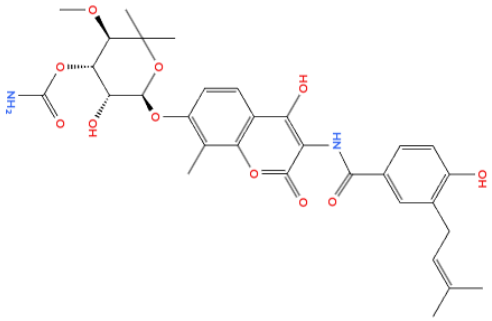	$C_{31}H_{36}N_2O_{11}$
10	Calophyllolide	5281392	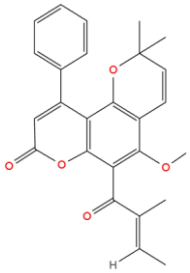	$C_{26}H_{24}O_5$
11	Chartreusin	5281394	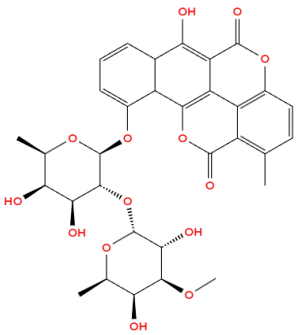	$C_{32}H_{32}O_{14}$
12	Frutinone A	441965	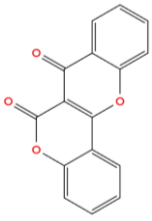	$C_{16}H_8O_4$

13	Hydrangenol	119199	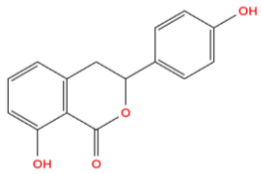	$C_{15}H_{12}O_4$
14	Phyllocoumarin	4257095	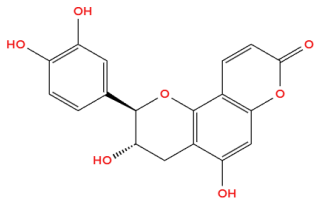	$C_{18}H_{14}O_7$

The 3D structures of the compounds were retrieved from the PubChem database (https://pubchem.ncbi.nlm.nih.gov) in SDF format and subsequently converted to PDB format using BIOVIA Discovery Studio 2024 Client 24.1 [25], and subsequently transformed into PDBQT format using AutoDock Vina for molecular docking with the selected fibronectin-FnBP-A complex models.

2.4. Molecular docking study

AutoDock4 and AutoDock Vina were used to perform molecular docking of the selected coumarin ligands with the fibronectin-FnBP-A complex models. AutoDock4 applies a genetic algorithm with local search to identify and refine optimal binding poses based on binding energy [27], whereas AutoDock Vina employs gradient-based optimisation combined with stochastic global search to generate and refine poses according to free-energy gradients [28, 29].

For each protein-ligand docking simulation, the binding-site coordinates were defined based on predictions generated by PrankWeb for each specific model (Table 2), using a grid box size of 30×30×30. AutoDock4 simulations were carried out with 100 genetic algorithm runs, a population size of 150, and a maximum of 27,000 generations. Docking with AutoDock Vina was performed with an exhaustiveness of 12, retaining up to 20 poses within an energy range of 3 kcal/mol. The optimal binding pose was selected based on the lowest binding energy together with RMSD lower and upper bound values below 2 Å. Docking performance was evaluated using ROC curves and AUC values, while

vancomycin HCl was used as the positive control to identify ligands with the strongest binding potential.

The resulting interactions between the ligands and the complexes were subsequently visualised and analysed using PyMOL Molecular Graphics System 3.1.6.1 [30] and BIOVIA Discovery Studio 2024 Client 24.1 [25].

2.5. Pharmacological analysis

The selected coumarin ligands were subjected to pharmacokinetic analysis based on key parameters, including absorption, metabolism, toxicity, and compliance with Lipinski's Rule of Five [31, 32]. Drug-likeness and molecular properties were predicted using Molsoft ICM v3.9-4 (https://www.molsoft.com/), while ADMETlab 3.0 was used to assess ADMET profiles.

3. Results and discussion

3.1. FnBP-A-fibronectin complex binding-site identification

FnBP-A-fibronectin complex structures 2RKZ, 2RKY, 3CAL, and 2RL0 were determined using X-ray crystallography, with respective resolutions of 2.00 Å, 1.8 Å, 1.7 Å, and 2.00 Å (Fig. 1), indicating high structural quality suitable for subsequent computational studies.

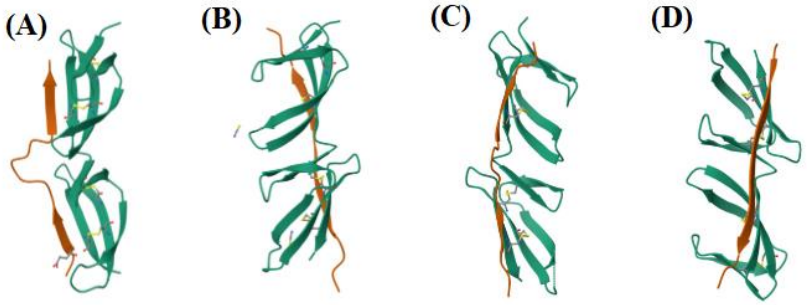

Fig. 1. Structural models of the FnBP-A (orange)-fibronectin (green) complex in **different crystallographic models. (A)** Model 2RKZ; **(B)** Model 2RKY; **(C)** Model 3CAL; **(D)** Model 2RL0.

Among the four complex models investigated, 2RKZ was selected as the primary model. It represents the interaction between a FnBR region of FnBP-A and the F2–F3

modules of fibronectin and was previously used to characterize the β-zipper binding mechanism [24]. The remaining models, 2RKY, 3CAL, and 2RL0, depict interactions between other FnBR regions and fibronectin modules and were used as comparative controls supporting a similar β-zipper mechanism. All four models were analyzed using PrankWeb to predict protein–protein interaction sites. Multiple regions were identified, and the most prominent sites were selected based on the highest binding scores and interaction probabilities (Table 2).

Table 2. The binding scores, probabilities, and coordinates of the binding site of four models (2RKZ, 2RKY, 3CAL, and 2RL0) predicted by PrankWeb.

Model	Binding score	Probability (%)	Coordination of the binding site		
			X	***Y***	***Z***
2RKZ	39.24	95.6	-8.7694	-24.2743	-25.7182
2RKY	15.05	74.9	8.058	21.7197	26.4707
3CAL	16.44	77.9	18.6476	-1.3542	10.3012
2RL0	18.79	82.3	28.5986	-24.5725	-4.5504

3.2. Docking results of ligands with the FnBP-A-fibronectin complex

The coumarin ligands were docked into predicted binding sites using AutoDock4 and AutoDock Vina based on prior binding-site coordinates. Docking of 14 ligands with four protein models (2RKZ, 2RKY, 3CAL, and 2RL0) showed that the coumarins interacted with both proteins in the complex (Tables 3 and 4).

Table 3. Docking results of 14 coumarin compounds and vancomycin HCl with 2RKZ, 2RKY, 3CAL, and 2RL0 by AutoDock Vina.

Compounds	Binding affinity (kcal/mol)			
	2RKZ	***2RKY***	***3CAL***	***2RL0***
Coumarin	-6.4	-7.2	-6.5	-6.1
Aculeatin	-6	-4.9	-6	-6.9
Cichoriin	-7.5	-6.3	-6.8	-8.5

Esculin	-7.1	-6.2	-6.7	-8.7
Fraxin	-7.7	-6.2	-6.7	-7.4
Oximes 3A	-6.4	-5.6	-7.7	-7.3
Oximes 3E	-6.1	-5.6	-6.7	-7.5
Osthole	-6.7	-5.9	-6.4	-7.3
Novobiocin	-8.4	-7.7	-7.8	-9.4
Calophyllolide	-8.1	-6.6	-7	-7.5
Chartreusin	-8.1	-7.2	-8.9	-7.5
Frutinone A	-7.8	-6.7	-10.2	-9.7
Hydrangenol	-8.6	-6.8	-7.3	-8.5
Phyllocoumarin	-8	-7.1	-8.2	-9.8
Positive control				
Vancomycin HCl	-8.5	-7.2	-7.7	-9.1

Table 4. Docking results of 14 coumarin compounds and vancomycin HCl with 2RKZ, 2RKY, 3CAL, and 2RL0 by AutoDock4.

Compounds	**Binding affinity (kcal/mol)**			
	2RKZ	***2RKY***	***3CAL***	***2RL0***
Coumarin	-7.85	-4.58	-6.71	-7.57
Aculeatin	-9.49	-6.70	-8.28	-7.87
Cichoriin	-7.37	-5.62	-8.68	-7.45
Esculin	-6.65	-5.80	-7.69	-7.49
Fraxin	-7.57	-6.17	-9.37	-8.40
Oximes 3A	-7.90	-7.62	-7.62	-8.19
Oximes 3E	-5.03	-4.33	-6.19	-6.18
Osthole	-7.20	-5.72	-7.44	-7.38

Novobiocin	-6.34	-6.77	-6.02	-5.52
Calophyllolide	-6.97	-5.85	-7.68	-6.79
Chartreusin	-6.95	-5.34	-6.46	-7.42
Frutinone A	-6.98	-5.60	-7.11	-6.78
Hydrangenol	-7.65	-4.53	-6.73	-7.32
Phyllocoumarin	-5.75	-4.48	-7.09	-7.21
Positive control				
Vancomycin HCl	-8.1	-6.92	-7.56	-8.02

ROC and AUC analyses indicated superior classification performance of AutoDock4 compared with AutoDock Vina. Across all four models (2RKZ, 2RKY, 3CAL, and 2RL0), AutoDock4 consistently achieved an AUC of 1.0 at a binding-energy threshold of −7 kcal/mol, whereas AutoDock Vina reached an AUC of 1.0 only in 2RL0 and 2RKY, with lower values in 3CAL (0.857) and 2RKZ (0.8). However, AUC values mainly reflect internal consistency rather than biological relevance. Therefore, vancomycin HCl was used as a positive reference, as it is recommended for treating septic arthritis caused by MRSA and MSSA, with MIC values below 2 μg/ml according to CLSI and EUCAST standards [33–36]. Ligand candidates were selected by comparing binding energies with vancomycin HCl across both docking engines using a z-mean consensus scoring approach.

Comparison of docking results across four models showed that chartreusin, frutinone A, phyllocoumarin, and novobiocin exhibited stronger binding affinities than vancomycin HCl, indicating their potential as alternative candidates. However, docking-derived binding affinities mainly reflect enthalpic contributions and do not account for entropic effects, and should therefore be interpreted as relative rather than absolute thermodynamic values.

3.3. Interaction analysis of ligands with the FnBP-A-fibronectin complex

Interaction analysis using BIOVIA Discovery Studio revealed that chartreusin, frutinone A, phyllocoumarin, and novobiocin formed interactions with both FnBP-A and fibronectin in all four structural models (2RKZ, 2RKY, 3CAL, and 2RL0).

Chartreusin interacted with fibronectin and FnBP-A in models 2RKZ, 2RKY, and 2RL0 (Table 5). In 2RKZ, hydrogen bonds were formed with B: ALA107, A: GLY131, B: GLY142, and F: GLU145 of fibronectin, as well as N: THR524 of FnBP-A (Fig. 2A). These interactions suggest favourable enthalpic contributions and enhanced complex stability. In 2RKY, hydrogen bonding occurred at A: ASP157, A: LYS172, and A: GLN175 of fibronectin and D: GLU524 of FnBP-A (Fig. 2B). In 2RL0, chartreusin formed hydrogen bonds with F: ARG197, A: GLN226, and A: GLU240 of fibronectin and hydrophobic contacts with G: VAL640 of FnBP-A. Additional electrostatic and hydrophobic interactions further contributed to stabilisation. However, unfavourable interactions observed in 2RKY and 2RL0 suggest steric or electrostatic clashes that may reduce complex stability (Figs. 2B and 2C).

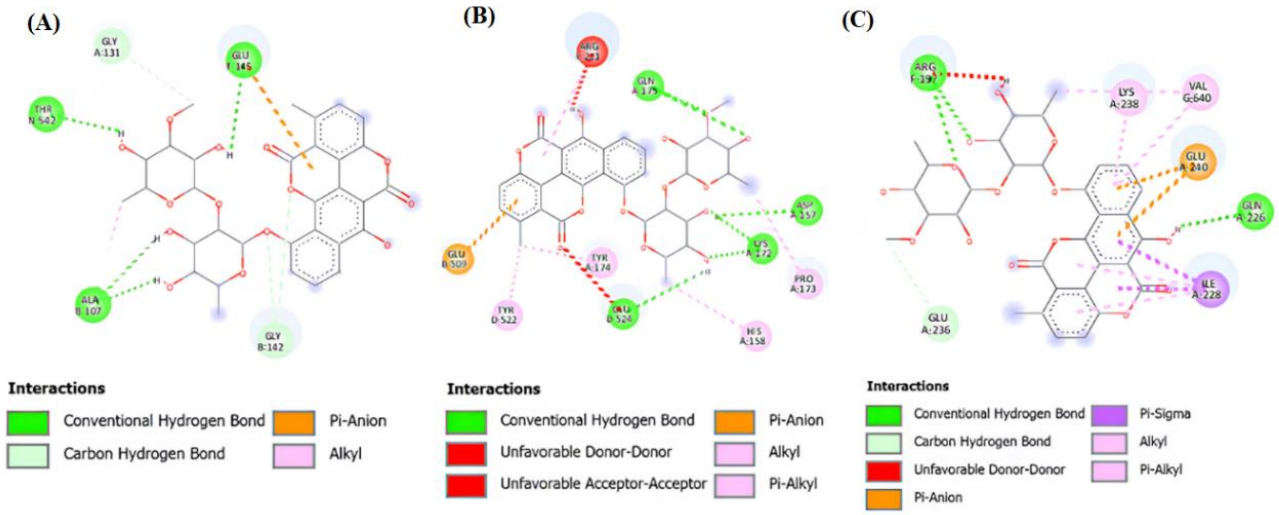

(D) (E) (F)

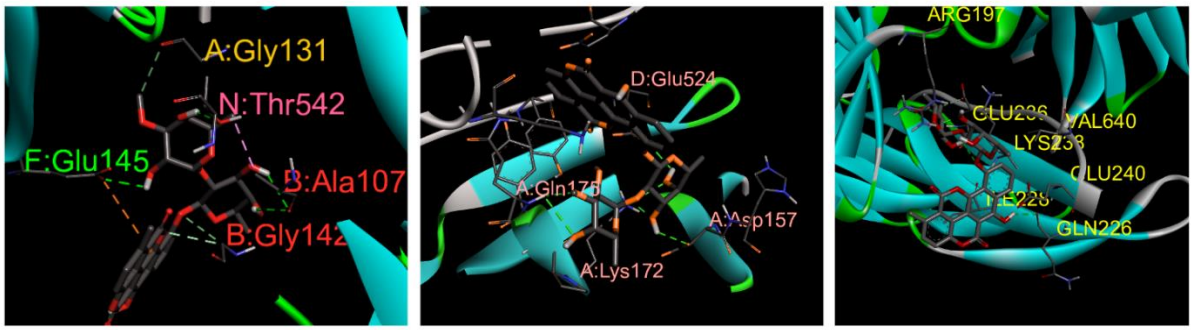

Fig. 2. Interaction between chartreusin and 2RKZ (A, D), 2RKY (B, E), and 2RL0 (C, F).

Table 5. Interaction between chartreusin and 2RKZ, 2RKY, 3CAL, and 2RL0.

Model	Binding affinity (kcal/mol)	Interaction			
		Protein	***Residue***	***Bond***	***Length (Å)***
2RKZ	-8.1	Fibronectin	B: ALA107	Hydrogen bond	3.055, 2.56
			F: GLU145		1.92
			B: GLY142		3.71, 3.31
			A: GLY131		3.46
			F: GLY145	Electrostatic interaction	4.8
			B: ALA107	Hydrophobic interaction	3.47
		FnBP-A	N: THR542	Hydrogen bond	2.438
2RKY	-7.2	Fibronectin	A: LYS172	Hydrogen bond	1.98, 2.54
			A: GLN175		3.09, 2.33
			A: ASP157		2.86
			A: PRO173	Hydrophobic interaction	3.99
			A: HIS158		5.21
			A: TYR174		4.45
			C: ARG221		4.93
		FnBP-A	D: GLU524	Hydrogen bond	2.6
			B: GLU509	Electrostatic interaction	4.26
			D: TYR522	Hydrophobic interaction	3.79
3CAL	-8.9	Fibronectin	C: ASN108	Hydrogen bond	2.72, 2.66

			C: ASN141		2.38
			C: LEU139		3.21
			C: CYS138		3.28
			A: ARG109	Electrostatic interaction	4.45, 3.72
			A: GLU82	Hydrophobic interaction	4.33
			C: ASN141		3.73
			A: LYS118		5.3
			A: ILE119		4.59
			C: ILE119		5.18
2RL0	-7.5	Fibronectin	F: ARG197	Hydrogen bond	1.98, 2.6
			A: GLN226		2.3
			A: GLU236		3.42
			A: GLU240	Electrostatic interaction	3.59, 3.8
			A: ILE228	Hydrophobic interaction	3.35, 3.7
			A: LYS238		4.67
		FnBP-A	G: VAL640	Hydrophobic interaction	4.9

Frutinone A interacted with both proteins in models 2RKZ and 3CAL (Table 6). In model 2RKZ, hydrogen bonds were formed at A: GLY131 and B: GLY142 of fibronectin, and N: THR541 of FnBP-A. The stability of the complex was further supported by electrostatic and hydrophobic interactions (Fig. 3A). In model 3CAL, hydrogen bonds were observed at A: SER103 and C: SER103 of fibronectin, while hydrophobic interactions with D: HIS665 were detected in FnBP-A (Fig. 3B). The formation of fewer interactions in model 3CAL indicates that its complex with the ligand is likely to be less stable than that of model 2RKZ.

Table 6. Interaction between frutinone A and 2RKZ, 2RKY, 3CAL, and 2RL0.

Model	**Binding affinity (kcal/mol)**	**Interaction**			
		Protein	***Residue***	***Bond***	***Length (Å)***
2RKZ	-7.8	Fibronectin	A: GLY131	Hydrogen bond	3.5
			B: GLY142		3.77
			F: GLU145	Electrostatic interaction	4.1, 3.23, 4.1

			B: ALA107	Hydrophobic interaction	4.92
			A: PRO126		5.4
			F: LEU139		3.68
		FnBP-A	N: THR541	Hydrogen bond	2.64
2RKY	-6.7	Fibronectin	C: GLN175	Hydrogen bond	3.1
			A: ARG221		2.37
			C: TYR174	Hydrophobic interaction	4.94
			C: PRO173		5.11
			C: ALA159		4.52
3CAL	-10.2	Fibronectin	A: SER103	Hydrogen bond	2.37, 2.31
			C: SER103		2.56
			A: ASP91	Electrostatic interaction	4.91
			C: ALA107	Hydrophobic interaction	5.1, 4.07
			A: THR105		3.2, 3.8
			C: THR105		3.4, 3.54
		FnBP-A	D: HIS665	Hydrophobic interaction	5.78
2RL0	-9.7	Fibronectin	F: ARG210	Hydrogen bond	3.0434
			K: TYR164		2.86
			K: PRO173		3.32
			F: ASP213	Electrostatic interaction	3.45
			F: THR207	Hydrophobic interaction	3.48
			K: TRP170		5.63, 5.62
			K: LYS172		4.1
			K: ALA160		4.75

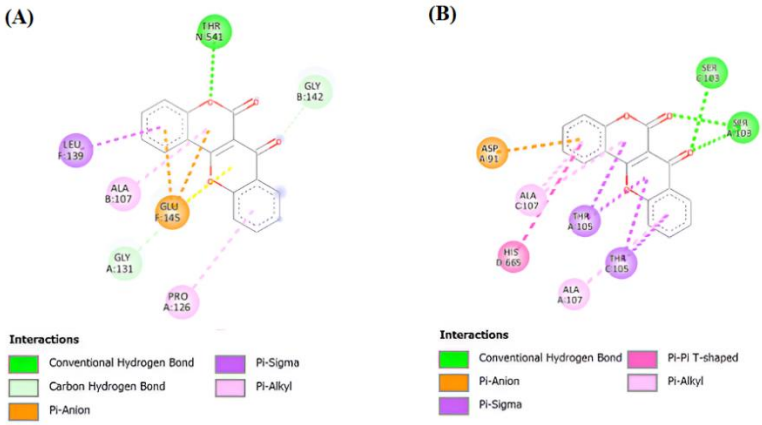

(C) (D)

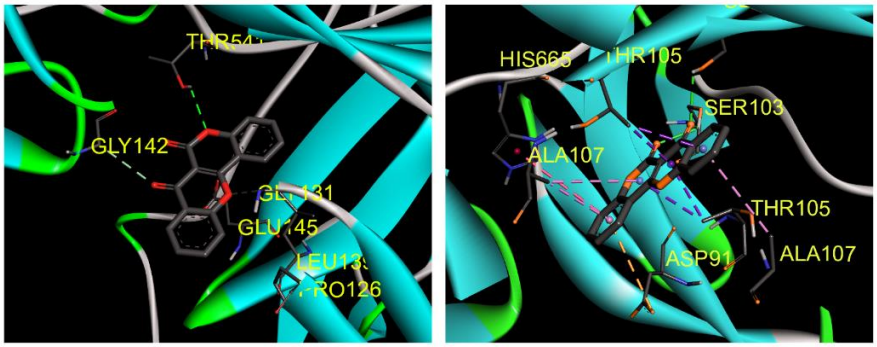

Fig. 3. Interaction between frutinone A and 2RKZ (A, C) and 3CAL (B, D).

Phyllocoumarin interacted with both target proteins in models 2RKY and 2RL0 (Table 7). In 2RKY, hydrogen bonds were formed at A: ARG197 and A: THR193 of fibronectin and B: LYS510, B: GLY521, and D: GLU521 of FnBP-A (Fig. 4A), indicating strong interactions with FnBP-A. In 2RL0, hydrogen bonds were observed at A: ASN108, A: THR105, C: ASP91, and A: GLY142 of fibronectin, along with hydrophobic interactions with C: ILE119 of FnBP-A (Fig. 4B). Additional electrostatic and hydrophobic interactions further stabilised the complexes (Fig. 4). The greater number of interactions in 2RKY suggests stronger binding affinity and potential pharmacological advantage.

Table 7. Interaction between phyllocoumarin and 2RKZ, 2RKY, 3CAL, and 2RL0.

Model	Binding affinity (kcal/mol)	Interaction			
		Protein	***Residue***	***Bond***	***Length (Å)***
2RKZ	-8	Fibronectin	B: ASN108	Hydrogen bond	2.15
			A: GLY131		2.17
			B: THR105		2.4
			F: GLU145	Electrostatic interaction	3.7
			B: ALA107	Hydrophobic interaction	3.9, 5.4
			F: LEU139		5.34
2RKY	-7.1	Fibronectin	A: ARG197	Electrostatic interaction	3.98
			A: THR193	Hydrophobic interaction	3.78
		FnBP-A	B: LYS510	Hydrogen bond	2.77

			B: GLY512		3.5
			D: GLU521		3.34
			D: LYS523	Hydrophobic interaction	5.19
3CAL	-8.2	Fibronectin	A: ASN108	Hydrogen bond	2.91
			A: THR105		2.38
			C: ASP91		2.32
			A: GLY142		3.15
			C: ILE119	Hydrophobic interaction	5.24
			A: ALA107		4
2RL0	-9.8	Fibronectin	A: ASN108	Hydrogen bond	2.54
			A: THR105		3.6
			C: ASP91		3.56
			A: GLY142		3.48
			A: ALA107	Hydrophobic interaction	4.72
		FnBP-A	C: ILE119	Hydrophobic interaction	4.64

(A)

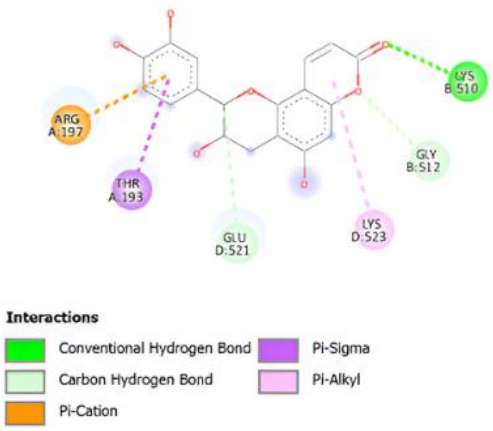

(B)

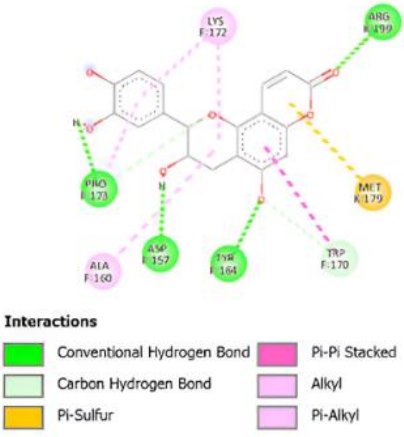

(C) **(D)**

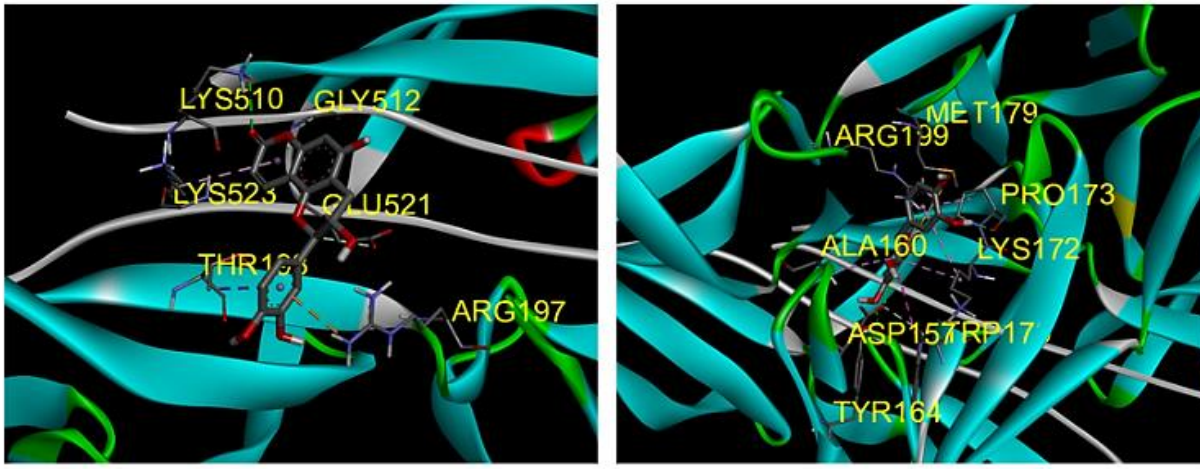

Fig. 4. Interaction between phyllocoumarin and 2RKY (A, C) and 2RL0 (B, D).

Novobiocin showed interactions with both proteins only in model 2RKZ. Hydrogen bonds were observed at F: ASN141, A: GLY131, B: GLY142, F: GLU145, and A: THR129 of fibronectin, as well as R: GLN534 of FnBP-A. Additional electrostatic and hydrophobic interactions further stabilised the ligand-protein complex (Fig. 5).

Table 8. Interaction between Novobiocin and 2RKZ, 2RKY, 3CAL and 2RL0.

Model	**Binding affinity (kcal/mol)**	**Interaction**			
		Protein	***Residue***	***Bond***	***Length (Å)***
2RKZ	-8.4	Fibronectin	F: ASN141	Hydrogen bond	2.1
			A: GLY131		2.03
			B: GLY142		3.36
			F: GLU145		3.53
			A: THR129		3.41
			F: GLU145	Electrostatic interaction	4.45
		FnBP-A	R: GLN534	Hydrogen bond	2.5
			R: LYS537	Hydrophobic interaction	4.33, 4.13

2RKY	-7.7	Fibronectin	C: ASP204	Hydrogen bond	2.26
			C: ASP219		2.85
			A: ASN220		2.32, 2.2, 2.82
			A: ASP204	Electrostatic interaction	3.71, 3.94
			C: LYS217	Hydrophobic interaction	4.8
3CAL	-7.8	Fibronectin	C: ILE119	Hydrogen bond	2.25
			A: GLY142		2.75
			C: LYS118	Hydrophobic interaction	3.84
			A: ILE119		4.97
			C: ILE119		5.34, 5.28
			C: LYS118		4.38, 4.05, 5.46
2RL0	-9.4	Fibronectin	K: TYR164	Hydrogen bond	2.96
			K: GLU171		2.86
			K: ASP157		2.31
			B: GLY233		2.77
			K: PRO173		3.41
			F: THR207		2.98
			F: ASP213	Electrostatic interaction	3.6
			F: THR207		3.35
			K: LYS172	Hydrophobic interaction	4.5
			K: PRO173		4.51
			F: ARG210		3.91
			K: TYR174		5.11
			K: ALA160		4.73
			K: LYS172		4.87

(A) **(B)**

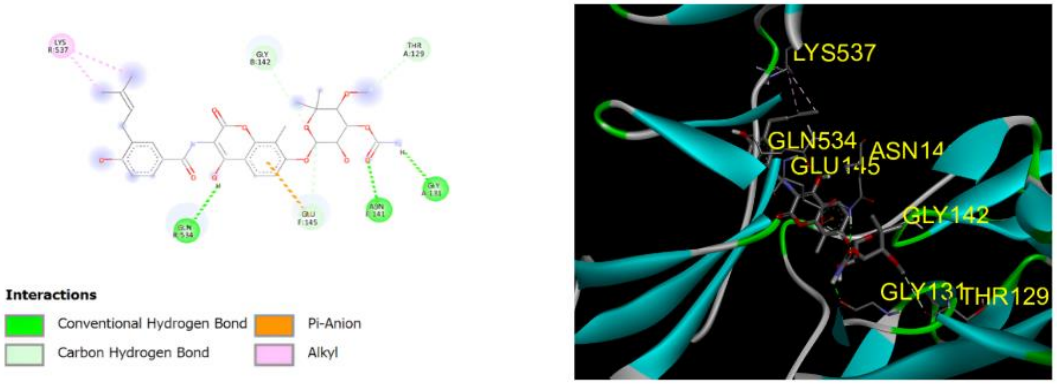

Fig. 5. Interaction between novobiocin (A) and 2RKZ (B).

Importantly, residues B: ALA107 and F: GLU145 were consistently involved in the interactions of all four ligands with model 2RKZ. This consistent involvement indicates that these residues occupy key positions within the binding pocket, playing an important role in the formation and stabilisation of the ligand-protein complex. Therefore, ALA107 and GLU145 may serve as potential hot spots for ligand optimisation to enhance binding affinity and selectivity in future studies.

3.4. Pharmacological analysis results

Lipinski's Rule of Five was used in this study to evaluate the drug-likeness of four coumarin compounds with favourable docking results: chartreusin, frutinone A, phyllocoumarin, and novobiocin (Table 9).

Table 9. Lipinski's rule of five parameter results for chartreusin, frutinone A, phyllocoumarin, and novobiocin.

Compounds	MW (< 500 Da)	LogP (< 5)	HBD (< 5)	HBA (< 10)	MR (40-130)
Chartreusin	640.6	0.947	5	14	154.029
Frutinone A	264	2.59	0	4	70.397
Phyllocoumarin	342	1.77	4	7	85.627
Novobiocin	612	3.138	6	13	155.91

Frutinone A and phyllocoumarin satisfied all five criteria of Lipinski's Rule of Five. In contrast, chartreusin and novobiocin had molecular weights exceeding 500 Da, and their

numbers of hydrogen-bond donors and acceptors were also higher than the required limits. Their MR values were also above 130. Therefore, chartreusin and novobiocin are likely to be highly polar in the body, making it difficult for them to permeate cell membranes and reducing their oral bioavailability. Frutinone A and phyllocoumarin were selected for further ADMET analysis, including evaluation of absorption, distribution, metabolism, excretion, and toxicity (Table 10).

Table 10. ADMET parameters of frutinone A and phyllocoumarin.

Parameter		Frutinone A	Phyllocoumarin
Absorption	Caco-2 permeability coefficient (LogPapp)	-4.414	-6.084
	P-gp inhibitor	0.422	0.343
	P-gp substrate	0.28	0.149
	Human intestinal absorption (HIA)	0.649	0.453
	F (Bioavailability 30%)	0.606	0.404
Distribution	Blood-brain barrier permeability (BBB)	0.992	0.757
	Plasma protein binding (PPB) (%)	86.193	88.278
	Volume of distribution (VD)	-0.501	-0.574
Metabolism	CYP1A2 substrate	Non-substrate	Non-substrate
	CYP3A4 substrate	Substrate	Substrate
	CYP1A2 inhibitor	Non-inhibitor	Non-inhibitor
	CYP3A4 inhibitor	Non-inhibitor	Substrate
Excretion	T ½ (Half life)	2.125	1.2
	Clearance (CL)	1.588	1.923
Toxicity	hERG	Yes	Yes
	Human hepatotoxicity (H-HT)	No	Yes
	Skin sensitisation (LLNA)	No	No
	AMES toxicity (Ames)	No	No
	LD50 (mol/kg)	2.461	2.97

Absorption was evaluated using Caco-2 permeability (LogPapp), P-gp inhibition, P-gp substrate status, and human intestinal absorption (HIA). Frutinone A showed higher

HIA than phyllocoumarin, indicating better intestinal absorption potential. However, both compounds exhibited low Caco-2 permeability, suggesting limited passive diffusion across the intestinal epithelium. This limitation may be attributed to their structural features, particularly multiple aromatic rings, which increase hydrophobicity and reduce aqueous solubility. In addition, both compounds showed low P-gp inhibition and substrate indices, indicating a high likelihood of efflux from intestinal cells, which may further reduce intracellular accumulation. Their oral bioavailability was predicted to be moderate, suggesting that despite some absorption potential, these compounds may still face barriers as oral drugs and could be more suitable for non-oral routes of administration.

Distribution was evaluated using BBB permeability, PPB, and VD. Frutinone A and phyllocoumarin showed high BBB penetration (0.992 and 0.757), suggesting CNS exposure, particularly for frutinone A. Both had PPB below 90%, indicating moderate binding, while low VD suggests limited tissue distribution and a potential risk of systemic toxicity at high plasma levels. Overall, frutinone A may exert greater CNS effects than phyllocoumarin.

The metabolic potential of frutinone A and phyllocoumarin was evaluated based on key hepatic cytochrome P450 enzymes. Both compounds were neither substrates nor inhibitors of CYP1A2, indicating that they are not metabolised via this pathway and are unlikely to interfere with CYP1A2-dependent drug metabolism. In contrast, both were identified as substrates of CYP3A4, suggesting metabolism by this major hepatic enzyme and potential susceptibility to drug–drug interactions. Frutinone A showed no inhibitory activity toward CYP3A4, indicating a low risk of affecting the metabolism of co-administered drugs. However, phyllocoumarin acted as a CYP3A4 inhibitor, suggesting that it may alter the pharmacokinetics of CYP3A4-dependent drugs, potentially increasing drug exposure and toxicity.

Excretion of frutinone A and phyllocoumarin was evaluated using their half-life and clearance (CL) rates. Both compounds had relatively short half-lives, suggesting a

moderate elimination rate. Additionally, their clearance rates were at a moderate level, with phyllocoumarin indicating faster elimination than frutinone A.

Toxicity assessment included hERG inhibition, hepatotoxicity, skin sensitisation (LLNA), genotoxicity (AMES), and LD_{50}. Both compounds showed hERG inhibition potential, suggesting a risk of cardiac arrhythmia, while phyllocoumarin additionally exhibited hepatotoxicity. However, both were non-irritant and non-mutagenic. Their LD_{50} values were relatively low (2.461 g/kg for frutinone A and 2.97 g/kg for phyllocoumarin), indicating notable acute toxicity. Overall, frutinone A appears less toxic than phyllocoumarin but still warrants caution due to its potential cardiotoxicity.

Although ADMET analysis provided insight into absorption, permeability, and toxicity, this study did not assess off-target interactions due to its focus on FnBP-A docking and basic pharmacokinetic predictions. Therefore, potential off-target effects of these coumarin derivatives require further investigation, particularly during structural optimisation and in vitro validation.

4. Conclusions

The binding affinities of fourteen compounds towards the FnBP-A-fibronectin complex were evaluated using AutoDock4 and AutoDock Vina, with vancomycin HCl employed as the positive control, given its established clinical use in the treatment of bone and joint infections. Four compounds - chartreusin, frutinone A, phyllocoumarin, and novobiocin - met the selection criteria. Their interactions with four models (2RKZ, 2RKY, 3CAL, and 2RL0) were analysed and visualised using PyMOL and BIOVIA Discovery Studio, revealing interactions with both FnBP-A and fibronectin across models. Notably, in the primary model 2RKZ, all four compounds consistently interacted at B: ALA107 and F: GLU145, suggesting key roles in ligand recognition and complex stabilisation.

The pharmacokinetic characteristics of chartreusin, frutinone A, phyllocoumarin, and novobiocin were further assessed using Lipinski's Rule of Five and ADMET profiling. Due to violations of Lipinski's criteria, chartreusin and novobiocin were not included in subsequent ADMET analyses. In contrast, ADMET evaluation of frutinone A and

phyllocoumarin indicated that both compounds may possess drug-like potential, although limitations in absorption and toxicity suggest that they may be more suitable for non-oral administration.

Frutinone A has been widely studied, whereas data on the in vivo or clinically relevant properties of phyllocoumarin remain limited. The present findings suggest that phyllocoumarin may serve as a promising lead compound against *S. aureus* infections. Although chartreusin and novobiocin were not included in ADMET analysis, previous reports and consistent docking results from both platforms indicate that they also warrant further experimental evaluation, particularly for bone and joint infections.

CRediT author statement

Thu Minh Nguyen: Methodology, Data analysis, and Writing; Luan Luong Chu: Conceptualisation, Methodology, Data analysis, Writing - Reviewing and Editing.

COMPETING INTERESTS

The authors declare that there is no conflict of interest regarding the publication of this article.

REFERENCES

[1] C. Heilmann (2011), "Adhesion mechanisms of staphylococci", *Advances in Experimental Medicine and Biology*, **715**, pp.105-123, DOI: 10.1007/978-94-007-0940-9_7.

[2] T.J. Foster (2019), "Surface proteins of *Staphylococcus aureus*", *Microbiology Spectrum*, **7(4)**, DOI: 10.1128/microbiolspec.gpp3-0046-2018.

[3] J.M. Patti, B.L. Allen, M.J. McGavin, et al. (1994), "MSCRAMM-mediated adherence of microorganisms to host tissues", *Annual Review of Microbiology*, **48**, pp.585-617, DOI: 10.1146/annurev.mi.48.100194.003101.

[4] T.J. Foster (2016), "The remarkably multifunctional fibronectin binding proteins of *Staphylococcus aureus*", *European Journal of Clinical Microbiology & Infectious Diseases*, **35**, pp.1923-1931, DOI: 10.1007/s10096-016-2763-0.

[5] N.V. An, L.H.L. Hai, V.H. Luong, et al. (2024), "Antimicrobial resistance patterns of *Staphylococcus aureus* isolated at a general hospital in Vietnam between 2014 and 2021", *Infection and Drug Resistance*, **17**, pp.259-273, DOI: 10.2147/IDR.S437920.

[6] D.S. Reddy, M. Kongot, S.P. Netalkar, et al. (2018), "Synthesis and evaluation of novel coumarin-oxime ethers as potential anti-tubercular agents: Their DNA cleavage ability and BSA interaction study", *European Journal of Medicinal Chemistry*, **150**, pp.864-875, DOI: 10.1016/j.ejmech.2018.03.042.

[7] M.F. Borges, F.M. Roleira, N.J. Milhazes, et al. (2009), "Simple coumarins: Privileged scaffolds in medicinal chemistry", *Frontiers in Medicinal Chemistry*, **4**, pp.23-85, DOI: 10.2174/97816080520731090401.

[8] A. Onder (2020), "Anticancer activity of natural coumarins for biological targets", *Studies in Natural Products Chemistry*, **67**, pp.85-109, DOI: 10.1016/B978-0-12-818569-3.00007-7.

[9] D. Srikrishna, C. Godugu, P.K. Dubey (2018), "A review on pharmacological properties of coumarins", *Mini-Reviews in Medicinal Chemistry*, **18(2)**, pp.113-141, DOI: 10.2174/1389557516666160801094919.

[10] A.H.L. Tuan, D.C. Kim, W. Ko, et al. (2017), "Anti-inflammatory coumarins from *Paramignya trimera*", *Pharmaceutical Biology*, **55(1)**, pp.1195-1201, DOI: 10.1080/13880209.2017.1296001.

[11] J. Sharifi-Rad, N. Cruz-Martins, P. López-Jornet, et al. (2021), "Natural coumarins: Exploring the pharmacological complexity and underlying molecular mechanisms", *Oxidative Medicine and Cellular Longevity*, **2021**, DOI: 10.1155/2021/6492346.

[12] Q. Xie, X. Wang, X. Wang, et al. (2005), "Design, synthesis, and bioavailability evaluation of coumarin-based prodrug of meptazinol", *Bioorganic & Medicinal Chemistry Letters*, **15(22)**, pp.4953-4956, DOI: 10.1016/j.bmcl.2005.08.016.

[13] G.E. Escudero, C.H. Laino, G.A. Echeverria, et al. (2016), "Improving the antidepressant action and the bioavailability of sertraline by co-crystallization with

coumarin 3-carboxylate: Structural determination", *Chemico-Biological Interactions*, **249**, pp.46-55, DOI: 10.1016/j.cbi.2016.03.010.

[14] M. Kumagai, A. Watanabe, I. Yoshida, et al. (2018), "Evaluation of aculeatin and toddaculin isolated from *Toddalia asiatica* as anti-inflammatory agents in LPS-stimulated RAW264 macrophages", *Biological & Pharmaceutical Bulletin*, **41(1)**, pp.132-137, DOI: 10.1248/bpb.b17-00607.

[15] H.E. Khalil, M.F. Abdelwahab, H.M. Ibrahim, et al. (2022), "Mechanistic insights into the ameliorative effect of cichoriin on diabetic rats-assisted with an *in silico* approach", *Molecules*, **27(21)**, DOI: 10.3390/molecules27217192.

[16] C. Liang, W. Ju, S. Pei, et al. (2017), "Pharmacological activities and synthesis of esculetin and its derivatives: A mini-review", *Molecules*, **22(3)**, DOI: 10.3390/molecules22030387.

[17] W.K. Whang, H.S. Park, I. Ham (2005), "Natural compounds, fraxin and chemicals structurally related to fraxin protect cells from oxidative stress", *Experimental and Molecular Medicine*, **37(5)**, pp.436-446, DOI: 10.1038/emm.2005.54.

[18] M. Sun, M. Sun, J. Zhang (2021), "Osthole: An overview of its sources, biological activities, and modification development", *Medicinal Chemistry Research*, **30**, pp.1767-1794, DOI: 10.1007/s00044-021-02775-w.

[19] C. Anderle, M. Stieger, M. Burrell, et al. (2008), "Biological activities of novel gyrase inhibitors of the aminocoumarin class", *Antimicrobial Agents and Chemotherapy*, **52(6)**, pp.1982-1990, DOI: 10.1128/AAC.01235-07.

[20] V.L. Nguyen, C.T. Truong, B.C.Q. Nguyen, et al. (2017), "Anti-inflammatory and wound healing activities of calophyllolide isolated from *Calophyllum inophyllum* Linn.", *PLOS ONE*, **12(10)**, DOI: 10.1371/journal.pone.0185674.

[21] J.P. McGovren, G.L. Neil, S.L. Crampton, et al. (1977), "Antitumor activity and preliminary drug disposition studies on chartreusin (NSC 5159)", *Cancer Research*, **37(6)**, pp.1666-1672, DOI: 10.1016/j.chembiol.2005.04.017.

[22] R.S. Thelingwani, K. Dhansay, P. Smith, et al. (2012), “Potent inhibition of CYP1A2 by Frutinone A, an active ingredient of the broad spectrum antimicrobial herbal extract from *P. fruticosa*. *Xenobiotica*”, **42(10)**, pp.989-1000, DOI: 10.3109/00498254.2012.681077.

[23] H. Matsuda, H. Shimoda, J. Yamahara, et al. (1999), “Effects of phyllodulcin, hydrangenol, and their 8-O-glucosides, and thunberginols A and F from *Hydrangea macrophylla* SERINGE var. *thunbergii* MAKINO on passive cutaneous anaphylaxis reaction in rats”, *Biological & Pharmaceutical Bulletin*, **22(8)**, pp.870-872, DOI: 10.1248/bpb.22.870.

[24] R.J. Bingham, E. Rudino-Pinera, N.A. Meenan, et al. (2008), “Crystal structures of fibronectin-binding sites from *Staphylococcus aureus* FnBPA in complex with fibronectin domains”, *Proceedings of The National Academy of Sciences of the United States of America*, **105(34)**, pp.12254-12258, DOI: 10.1073/pnas.0803556105.

[25] S. Goswami, S.P. Kollur, A. Nayak, et al. (2026). “Molecular docking and dynamics-based repurposing of Thalidomide and Lenalidomide for GSK-3β inhibition in AD”, *CNS & Neurological Disorders Drug Targets*, DOI: 10.2174/0118715273411602251130120518.

[26] L. Polak, P. Skoda, K. Riedlova, et al. (2025), “PrankWeb 4: A modular web server for protein-ligand binding site prediction and downstream analysis”, *Nucleic Acids Research*, **53(W1)**, pp.466-471, DOI: 10.1093/nar/gkaf421.

[27] G.M. Morris, R. Huey, W. Lindstrom, et al. (2009), “AutoDock4 and AutoDockTools4: Automated docking with selective receptor flexibility”, *Journal of Computational Chemistry*, **30(16)**, pp.2785-2791, DOI: 10.1002/jcc.21256.

[28] O. Trott, A.J. Olson (2010), “AutoDock Vina: Improving the speed and accuracy of docking with a new scoring function, efficient optimization, and multithreading”, *Journal of Computational Chemistry*, **31(2)**, pp.455-461, DOI: 10.1002/jcc.21334.

[29] J. Eberhardt, D. Santos-Martins, A.F. Tillack, et al. (2021), "AutoDock Vina 1.2.0: New docking methods, expanded force field, and python bindings", *Journal of Chemical Information and Modeling*, **61(8)**, pp.3891-3898, DOI: 10.1021/acs.jcim.1c00203.

[30] S. Rosignoli, A. Paiardini (2022), "Boosting the full potential of PyMOL with structural biology plugins", *Biomolecules*, **12(12)**, DOI: 10.3390/biom12121764.

[31] C.A. Lipinski (2004), "Lead- and drug-like compounds: The rule-of-five revolution", *Drug Discovery Today: Technologies*, **1(4)**, pp.337-341, DOI: 10.1016/j.ddtec.2004.11.007.

[32] B. Jayaram, T. Singh, G. Mukherjee, et al. (2012), "Sanjeevini: A freely accessible web-server for target directed lead molecule discovery", *BMC Bioinformatics*, **13(17)**, DOI:10.1186/1471-2105-13-S17-S7.

[33] D.R. Osmon, E.F. Berbari, A.R. Berendt, et al. (2013), "Diagnosis and management of prosthetic joint infection: Clinical practice guidelines by the infectious diseases society of America", *Clinical Infectious Diseases*, **56(1)**, pp.e1-e25, DOI: 10.1093/cid/cis966.

[34] Clinical and Laboratory Standards Institute (CLSI), *Performance Standards for Antimicrobial Susceptibility Testing; CLSI Supplement M100*, Wayne, PA, USA.

[35] P. Gaur, V. Hada, R.S. Rath, et al. (2023), "Interpretation of antimicrobial susceptibility testing using European Committee on Antimicrobial Susceptibility Testing (EUCAST) and Clinical and Laboratory Standards Institute (CLSI) Breakpoints: Analysis of agreement", *Cureus*, **15(3)**, DOI: 10.7759/cureus.36977.

[36] J. Ariza, J. Cobo, J. Baraia-Etxaburu, et al. (2017), "Executive summary of management of prosthetic joint infections: Clinical practice guidelines by the Spanish Society of Infectious Diseases and Clinical Microbiology (SEIMC)", *Enfermedades Infecciosas Y Microbiologia Clinica,* **35(3)**, pp.189-195, DOI: 10.1016/j.eimc.2016.